Chemical Engineering Science 63 (2008) 4189 – 4202

Contents lists available at ScienceDirect

Chemical Engineering Science

journal homepage: www.elsevier.com/locate/ces

An experimental investigation of gas–liquid two-phase flow in single microchannel contactors

Jun Yue[a,b], Lingai Luo[b,*], Yves Gonthier[b], Guangwen Chen[a], Quan Yuan[a,*]

[a]Dalian Institute of Chemical Physics, Chinese Academy of Sciences, Dalian 116023, China
[b]LOCIE, Université de Savoie, Campus Scientifique, Savoie Technolac, 73376 Le Bourget-du-Lac cedex, France

ARTICLE INFO

Article history:
Received 25 May 2007
Received in revised form 22 April 2008
Accepted 22 May 2008
Available online 9 July 2008

Keywords:
Microchannel
Multiphase flow
Flow pattern
Taylor flow
Pressure drop

ABSTRACT

This paper describes two-phase flow pattern and pressure drop characteristics during the absorption of CO_2 into water in three horizontal microchannel contactors which consist of Y-type rectangular microchannels having hydraulic diameters of 667, 400 and 200 μm, respectively. With the help of a high-speed photography system, flow patterns such as bubbly flow, slug flow (including two sub-regimes, Taylor flow and unstable slug flow), slug-annular flow, churn flow and annular flow were observed in these microchannels. The applicability of the currently available correlations for describing flow pattern transitions in microchannels has been examined. Generally, the predicting performance of these correlations deteriorates as the channel diameter further reduces. Toward solving this discrepancy, an empirical correlation based on the superficial Weber numbers was developed to interpret the transition from Taylor flow to unstable slug flow in three microchannels. Taylor bubble formation process in microchannels was found to be in the squeezing regime at lower superficial liquid velocities (*Ca* ranging from 0.0019 to 0.029) while the transition to the dripping regime was observed at the highest superficial liquid velocity of 1.0 m/s. Lengths of Taylor bubbles formed in the squeezing regime can be well represented by the scaling relation proposed by Garstecki et al. [Formation of droplets and bubbles in a microfluidic T-junction—scaling and mechanism of break-up. Lab on a Chip, 6, 437–446]. For flow patterns including slug-annular flow, annular flow and churn flow, a simple analysis based on the separated flow model has been performed in order to reveal the observed effect of the superficial liquid velocity on two-phase frictional multiplier in the present microchannels. Then, reasonable correlations for the prediction of two-phase frictional pressure drop under these flow patterns were suggested.

1. Introduction

Gas–liquid microreactor featuring two-phase flow in micro-geometries has numerous advantages compared to its macroscale counterparts. Ultra high surface to volume ratio achieved in such microreactor due to the decrease of linear size to micron scale improves heat and mass transfer process. Meanwhile, a great reduction in the whole reactor volume offers itself inherent safety and production flexibility (Ehrfeld et al., 2000). As a result, great efforts have been seen in recent years in the use of gas–liquid microreactors for mass transfer operations and reactions processes (with or without catalyst involved), wherein applications such as gas absorption/desorption, gas–liquid catalytic hydrogenation, hydrogen peroxide synthesis and direct fluorination turned to be very promising (de Mas et al., 2003; Hessel et al., 2005; Inoue et al., 2007; Jähnisch et al., 2000; Kobayashi et al., 2004; Löb et al., 2004; Tegrotenhuis et al., 2000; Yeong et al., 2004; Yue et al., 2007).

According to two-phase contacting principle, gas–liquid microreactors can be mainly classified into three categories (Hessel et al., 2005): (1) micro-bubble column: gas and liquid flow co-currently in the same microchannel and gas is introduced into liquid through ways such as bubbling; (2) falling film microreactor: liquid films are created and stabilized in parallel microchannels by gravity and gas flows in the above free space, facilitating co-current or counter-current operation; (3) microreactor with phase interface stabilized by well-defined physical structures: gas and liquid flow co-currently or counter-currently in two adjacent microchannels which are separated by a mesh structure or employ an overlapping channel configuration. Thus, two-phase interface is formed and stabilized in

* Corresponding authors. Tel.: +33 4 79 75 81 93; fax: +33 4 79 75 81 44 (L. Luo); Tel.: +86 411 84 68 79 94; fax: +86 411 84 69 51 70 (Q. Yuan).
E-mail addresses: Lingai.Luo@univ-savoie.fr, yuej@dicp.ac.cn (L. Luo), qyuan@dicp.ac.cn (Q. Yuan).

0009-2509/$ - see front matter © 2008 Elsevier Ltd. All rights reserved.
doi:10.1016/j.ces.2008.05.032

these well-defined openings. When solid catalysts are involved in gas–liquid reactions performed in the above reactors, they can be integrated as thin films deposited on the inner walls of microchannels by methods such as wash-coating or sputtering. For the precise control of mass transfer operations or reaction processes in these microreactors, hydrodynamics of two-phase flow in these microgeometries should be thoroughly investigated in advance.

This paper deals with characteristics of two-phase flow in the gas–liquid microreactor of the first type, i.e. micro-bubble column. The basic unit of this reactor geometry can be simply a straight microchannel section for gas–liquid contacting. Through a reasonable design of the whole system, preferable flow patterns can be formed stably throughout this narrow microchannel, which can then be utilized to intensify simultaneously occurring mass transfer and reaction processes. When conceiving the design criterion for this reactor, two-phase flow pattern and pressure drop characteristics are two very important parameters.

Up to now, many researches have been conducted on gas–liquid two-phase flow in circular, rectangular and even triangular microchannels (Chen et al., 2002; Chung and Kawaji, 2004; Cubaud and Ho, 2004; Kawahara et al., 2002; Serizawa et al., 2002; Triplett et al., 1999a,b; Yue et al., 2004; Zhao and Bi, 2001a,b). Plenty of flow patterns with characteristics specific to microchannels have been observed and flow pattern maps based on coordinates of the superficial gas and liquid velocities have been proposed, where the widely used flow transition models or correlations in large pipes were generally in poor agreement with the obtained data in microchannels (Cubaud and Ho, 2004; Serizawa et al., 2002; Triplett et al., 1999a; Zhao and Bi, 2001a). A possible explanation for this deviation is a result of the predominance of surface tension in microchannels under most circumstances. In view of this fact, Akbar et al. (2003) proposed a Weber number based flow pattern map that can describe the currently available data for near-circular microchannels and air–water like fluid pairs satisfactorily. However, they highlighted a need to pursue studies on two-phase flow transition in microchannels having other geometrical configurations. Similar discrepancy has also been found during the analysis of pressure drop characteristics in microchannels, that is, traditional flow-pattern independent correlations based on the separated flow model or the homogenous flow model at least partly lose their predicting accuracy in microchannels. For example, with regard to the classic correlation of Lockhart and Martinelli (1949), some authors have noticed that there is a significant effect of mass flux on the measured two-phase frictional multiplier in microchannels (Chung and Kawaji, 2004; Yue et al., 2004), which means that the correlation of Lockhart and Martinelli should be properly modified in order to be applicable to microchannels. Besides, the successful application of the homogeneous flow model in microchannels depends on the choice of a proper two-phase mixture viscosity correlation. Kawahara et al. (2002) found that good predictions of two-phase frictional pressure drop of N_2–water flow in a 100 μm diameter circular microchannel could be obtained only with Dukler et al.'s (1964) model for the mixture viscosity. However, Yue et al. (2004) suggested that the viscosity correlation of Mcadams (1954) gave the least predicting error for pressure drop data of N_2–water flow in two rectangular microchannels with $d_h = 528$ and 333 μm. While the results of Triplett et al. (1999b) indicated that the viscosity correlation of Mcadams (1954) could only predict reasonably the experimental pressure drop data of air–water bubbly flow and slug flow in a 1.097 mm diameter circular microchannel at high superficial liquid Reynolds numbers where the homogeneous flow model might be well applicable. Consequently, generalized pressure drop correlations are not available for microchannels at present. This unavailability is mainly attributed to the complicated two-phase flow behavior occurring at microscale. Furthermore, for non-circular microchannels, the channel shape certainly has a role to play. For example, some authors have reported that bubble shape and its motion characteristics in non-circular microchannels are comparatively different from those observed in circular microchannels (Bi and Zhao, 2001; Cubaud and Ho, 2004; Zhao and Bi, 2001a). As a result, pressure drop characteristics in non-circular microchannels are thought to differ from those in circular ones to some extent, which still remains to be resolved.

From the above summary, it is obvious that more experiments are still needed in order to clarify the underlying mechanisms of flow pattern transition, as well as pressure drop characteristics in microchannels having different diameters and geometrical configurations. When there is simultaneous mass transfer process involved, two-phase hydrodynamics will be more complicated. Thus, in the present work, two-phase flow characteristics during the absorption of CO_2 into water in three single microchannel contactors containing Y-type rectangular microchannels with hydraulic diameters of 667, 400 and 200 μm, respectively, have been investigated. Two-phase flow patterns in these microchannels were recorded with the aid of a high-speed photography system and the corresponding pressure drop data were measured. First, the validity of the currently available flow transition correlations for microchannels were examined in the present contactors by further considering the effect of mass transfer on two-phase flow evolution along the microchannel and an empirical correlation was also proposed to describe the transition boundary between Taylor flow and unstable slug flow in three microchannels. Then, Taylor bubble formation mechanism, Taylor bubble length, and gas hold up data in Taylor flow were discussed, where the influences of inlet geometry and aspect ratio were demonstrated to some extent. Finally, pressure characteristics in three microchannels were analyzed with an emphasis on flow patterns including slug-annular flow, annular flow and churn flow. The observed effect of the superficial liquid velocity on the measured two-phase flow friction multiplier in these flow patterns was discussed on the basis of the separated flow model and gas–liquid flow behavior in rectangular geometries, whereafter relatively simple empirical correlations for the prediction of two-phase frictional pressure drop were suggested.

2. Experimental section

2.1. Single microchannel contactor design

In the present study, three single microchannel contactors were employed. As shown in Fig. 1(a), each contactor mainly contains a Y-type rectangular microchannel structure micromachined on the polymethyl methacrylate substrate (PMMA) and the hydraulic diameters of these microchannels are 667, 400 and 200 μm, respectively. The two side microchannels for the introduction of gas and liquid form an angle of 60° and distribute symmetrically with respect to the central axis of the main microchannel where gas–liquid mixing and mass transfer occur. All channels in each contactor have the same cross-sectional dimensions (see Table 1 for more detailed parameters). The sealing of the open microchannel plate was realized first by attaching a piece of transparent adhesive tape on its top and then by clamping it against a smooth PMMA plate through the bolting holes on the peripheries of the two plates. Outer fluids interfaced the microchannel structure through inlet and outlet plenums, thus forming a single microchannel contactor. This type of contactor will be referred as SMC I hereafter.

The second type of PMMA contactor shown in Fig. 1(b) is termed as SMC II and was employed for the purpose of measuring the equivalent pressure drop contributions in the side microchannel and the exit pipe during experiments with SMC I. We have demonstrated that this type of contactor is also suitable for the elimination of mass transfer end effects when studying gas–liquid mass transfer characteristics in the single microchannel contactor with $d_h = 667$ μm

(Yue et al., 2007). The only difference between SMC II and the corresponding SMC I is that in the former contactor design the main microchannel no longer exists and the side microchannels are thus directly connected with the outlet plenum. The other dimensions of inner structures remain the same as those given in Table 1.

2.2. Experimental setup

The present work deals with hydrodynamics of two-phase flow during the absorption of CO_2 into water in three main microchannels shown in Fig. 1(a). A schematic diagram of the experimental apparatus for the measurement of two-phase flow pattern and pressure drop is depicted in Fig. 2. It should be added that in our previous paper, two-phase flow characteristics for this system under some typical operational conditions have been investigated in SMC I with $d_h = 667\,\mu m$ (Yue et al., 2007). Therefore for this contactor one part of the data presented in this paper was actually taken from that work (Yue et al., 2007) and the other part of the data were collected in the current experimental setup under further extended operational conditions in order to explore more details of two-phase flow in this contactor.

a

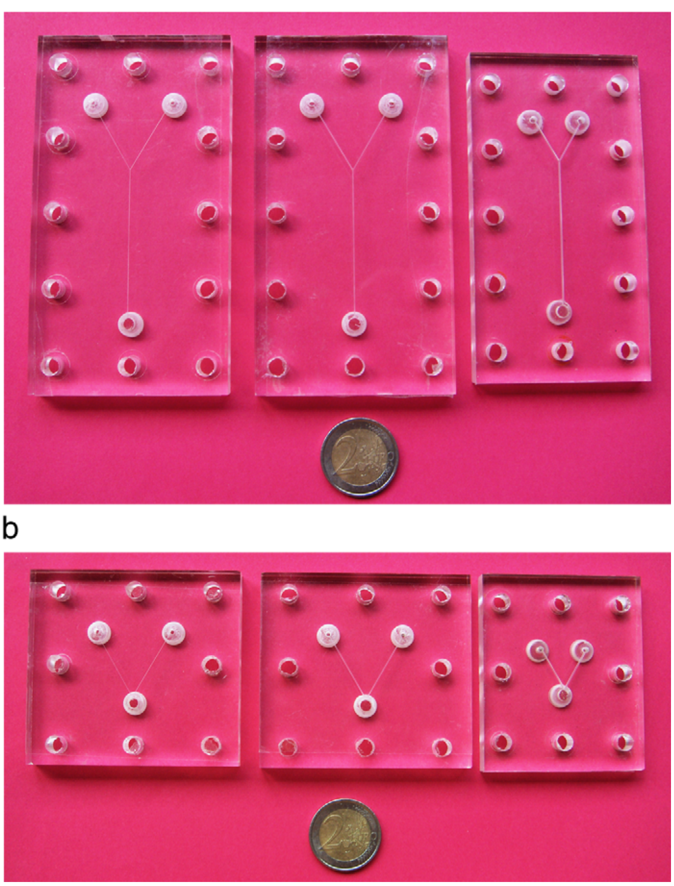

b

Fig. 1. Pictures of single microchannel contactors with $d_h = 200, 400$ and $667\,\mu m$, respectively (from left to right): (a) SMC I; (b) SMC II.

As shown in Fig. 2, gas phase consisted of pure CO_2 that was conveyed from a gas cylinder and its pressure was regulated by a pressure regulator. A filter installed thereafter served to remove possible contaminations in CO_2 stream. The precise flow rate of CO_2 input into one side microchannel in SMC I was set by one of several mass flow controllers with different flow ranges and a pressure transducer located in the gas feeding line just before the inlet plenum measured the corresponding gas inlet gauge pressure. Liquid used was boiled deionized water and was fed from the liquid tank into the other side microchannel by a positive displacement pump. In the liquid flow line, a filter was also employed and a buffer tank just after the pump was used to damp possible flow pulsations. The accurate liquid flow rate was measured by weighing method. After contacting horizontally in the main microchannel, two-phase mixture flowed out of the contactor and entered downward into a short polyethylene tube with an inner diameter of 4 mm before exiting into air. Two thermocouples (K-type) were located in the inlet plenums to measure the corresponding temperatures. All experiments were conducted under ambient conditions (0.1 MPa, 20 °C).

During CO_2–water flow in SMC I, two-phase flow images at the entrance and in the middle section of the main microchannel (3 cm from the entrance) were also recorded with the aid of a high-speed CCD camera placed above the contactor. A strong background illumination was provided by a fiber optic cold lamp positioned beneath the contactor. The captured frames were immediately transferred to a personal computer via a data acquisition system for later analysis. For Taylor flow, lengths of Taylor bubbles and liquid slugs at two locations were also measured from the corresponding images. Normally for each operational condition at least 10 images were analyzed and the measured lengths in all images were averaged together in order to obtain the final value. It was noticed that at a fixed operational condition, the difference among the lengths of Taylor bubbles or liquid slugs measured in one image or a series of images was insignificant, where the standard deviation was generally less than 5%.

In order to derive two-phase total pressure drop in the main microchannel of each SMC I, the corresponding SMC II shown in Fig. 1(b) was used while the other flow schematic was the same as that shown in Fig. 2.

2.3. Pressure data reduction

During two-phase flow experiments with SMC I, the measured inlet gauge pressure in the gas feeding line, $P_{\text{in, SMC I}}$, can be considered as a sum of the following pressure drop items: (a) $\Delta P_{\text{single phase}}$, pressure drop caused by gas single phase flow from the measuring point in the gas feeding line to the end of the side microchannel; (b) $\Delta P_{\text{entrance}}$, local pressure loss due to gas flow from the side microchannel into the main microchannel; (c) ΔP_T, two-phase total pressure drop in the main microchannel; (d) $\Delta P_{\text{expansion}}$, pressure drop caused by the expansion of two-phase mixture from the outlet

Table 1
Single microchannel contactor dimensions

Channel cross-section	Length of side microchannel (cm)	Length of main microchannel (cm)	Height (μm)	Width (μm)	Hydraulic diameter (μm)	Aspect ratio
Square	2.53	4.8	200	200	200	1
Square	2.53	4.8	400	400	400	1
Rectangular	1.5	4.8	1000	500	667	2

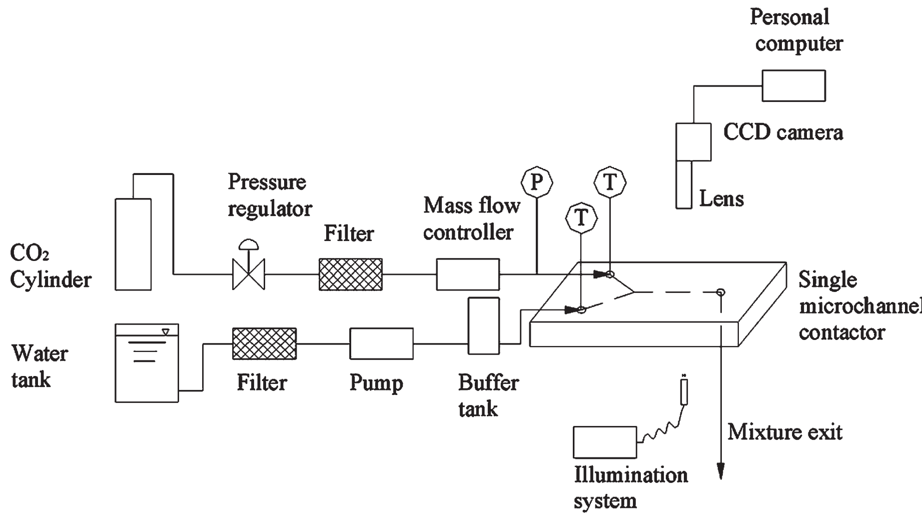

Fig. 2. Schematic of the experimental apparatus for the measurement of two-phase flow pattern and pressure drop in single microchannel contactors.

of the main microchannel to the exit 4 mm inner diameter pipe; (e) $\Delta P_{T,\,\mathrm{exit}}$, two-phase total pressure drop in the exit pipe.

When two-phase flow experiments were conducted by using SMC II under the same flow rates of gas and liquid as those for the corresponding SMC I, the measured inlet gauge pressure in the gas feeding line in this case, $P_{\mathrm{in,\,SMC\,II}}$, can be roughly estimated as the sum of the above-mentioned pressure items (a), (b), (d) and (e). This deduction is mainly based on the assumptions that single or two-phase hydrodynamic behaviors inside the corresponding sections for both contactors are almost identical and the variations in the average gas density and mass flow rate in both cases are negligible. Certainly these assumptions are highly idealized. However, it is thought that the method adopted here is still a reasonable way of estimating two-phase total pressure drop in the main microchannel, that is, ΔP_T can be calculated as

$$\Delta P_T = P_{\mathrm{in,\,SMC\,I}} - P_{\mathrm{in,\,SMC\,II}} \tag{1}$$

Consequently, the inlet and outlet gauge pressures in this microchannel, P_0 and P_1, can be derived as follows:

$$P_0 = P_{\mathrm{in,\,SMC\,I}} - (\Delta P_{\mathrm{single\ phase}} + \Delta P_{\mathrm{entrance}}) \tag{2}$$

$$P_1 = P_0 - \Delta P_T \tag{3}$$

The sum of pressure items (a) and (b), i.e., $(\Delta P_{\mathrm{single\ phase}}+\Delta P_{\mathrm{entrance}})$ located in the right side of Eq. (2), can be measured approximately by conducting single phase gas flow experiments in SMC II using the test facilities shown in Fig. 2. In detail, here liquid flow was stopped and the exit pipe was removed from the contactor, that is, only the prescribed flow rate of CO_2 was seen to flow through the side microchannel and then CO_2 stream vented directly from the outlet of the contactor into air. The reading provided by the pressure transducer can be regarded as a reasonable approximation of $(\Delta P_{\mathrm{single\ phase}} + \Delta P_{\mathrm{entrance}})$ under this specified operational condition.

3. Results and discussion

3.1. Two-phase flow patterns observed in the middle section of microchannels

Fig. 3 shows some representative images captured in the middle section of the microchannel with $d_h = 400\,\mu\mathrm{m}$ and some pictures in the microchannel with $d_h = 667\,\mu\mathrm{m}$ can be found elsewhere (Yue et al., 2007). Flow patterns such as bubbly flow, slug flow, slug-annular flow, annular flow and churn flow were identified, which was in accordance with the definitions of Triplett et al. (1999a). The superficial gas velocity, j_G shown in Fig. 3 was derived based on the gas density under the local pressure in the observation window with the assumptions of a linear pressure distribution and a constant gas mass flow rate along the microchannel. It should be noted that some errors in the determination of j_G will be incurred by these assumptions. According to our results on the absorption of CO_2 into water in the microchannel with $d_h = 667\,\mu\mathrm{m}$ (Yue et al., 2007), the variation in the mass flow rate of CO_2 along the microchannel was generally less than 10%. However, the significant reduction in the gas mass flow rate along the microchannel was also noticed at the lowest gas flow rate and the highest liquid flow rate fed into the system, for example, the variation sometimes amounted to as high as 40%. In the present experiments, the operational ranges were greatly extended in order to explore more details of possible two-phase flow pattern in microchannels. Therefore, for bubbly flow and Taylor flow shown in Figs. 3(a)–(d) which were observed at relatively low superficial gas velocities, a significant overestimation of j_G was expected. For other flow patterns occurring at relatively high superficial gas velocities, the variation of the gas mass flow rate was negligible and therefore j_G derived on the above assumptions was very close to the actual value in the microchannel.

In the present study, bubbly flow was observed at relatively high j_L and the lowest j_G, which was characterized by the dispersion of spherical bubbles in a continuous liquid phase. These small bubbles were more likely to coalesce due to the velocity differences among them (Fig. 3(a)). A further increase of j_G at the same j_L in bubbly flow caused the bubble to grow and flow in a more regular way, that is, the distance between every two bubbles was nearly equal and coalescence could not be seen any more (Fig. 3(b)). Another interesting phenomenon was that bubbles tended to flow along one side wall of the microchannel. When j_G was increased to a certain extent, the size of the bubble approached the microchannel width or height. Then the flow transition to slug flow began.

In slug flow, two sub-regimes were found (Yue et al., 2007): (1) Taylor flow emerged when j_G was relatively small. At rather low j_G and j_L, both Ca and Re_L were so small that the interfacial force was large enough to maintain the hemispheric shapes of Taylor bubble caps (Fig. 3(c)). At high j_G and j_L, both Ca and Re_L increased significantly and the effect of inertia began to play an important role. As

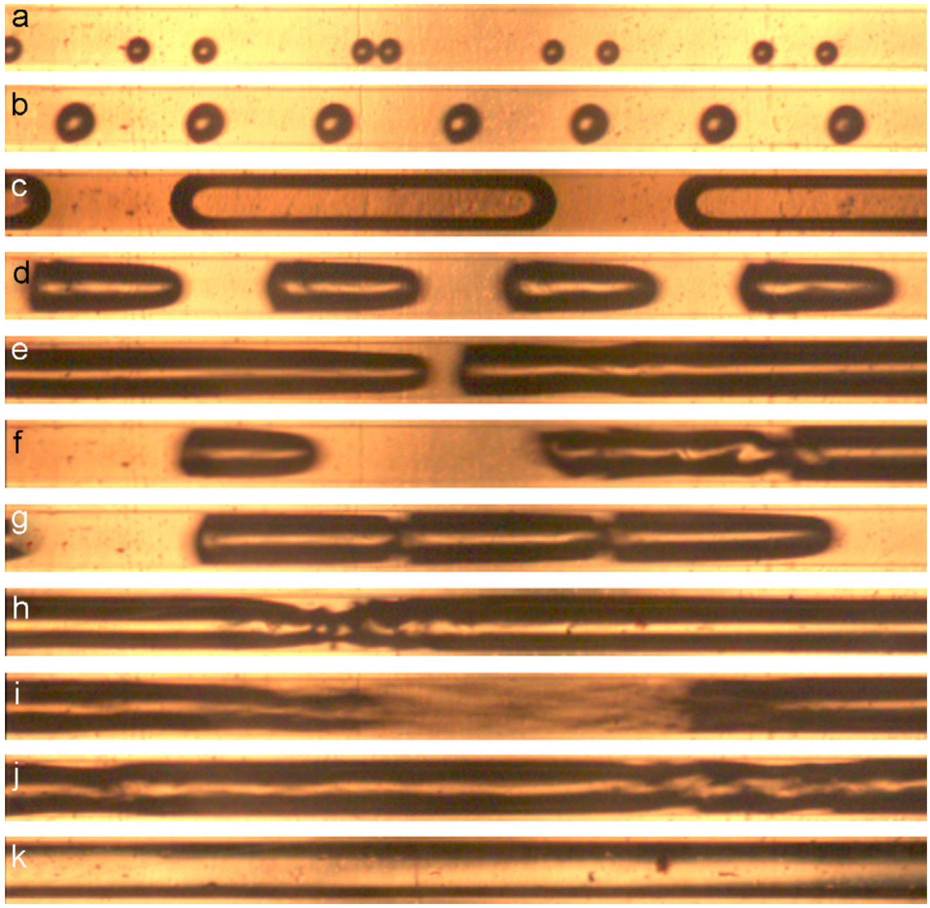

Fig. 3. Typical images encountered during CO_2–water flow in the microchannel with $d_h = 400\,\mu m$ (flow direction is from left to right and the observation point is at a distance of 3 cm from the entrance): (a) bubbly flow ($j_G = 0.16$ m/s, $j_L = 1.0$ m/s); (b) bubbly flow ($j_G = 0.29$ m/s, $j_L = 1.0$ m/s); (c) Taylor flow ($j_G = 0.16$ m/s, $j_L = 0.04$ m/s, $Ca = 0.0028$, $Re_L = 80$); (d) Taylor flow ($j_G = 1.28$ m/s, $j_L = 1.0$ m/s, $Ca = 0.031$, $Re_L = 913$); (e) unstable slug flow ($j_G = 1.74$ m/s, $j_L = 0.51$ m/s); (f) unstable slug flow ($j_G = 2.14$ m/s, $j_L = 0.51$ m/s); (g) bubble-train slug flow ($j_G = 2.07$ m/s, $j_L = 1.0$ m/s); (h) slug-annular flow ($j_G = 7.51$ m/s, $j_L = 0.20$ m/s); (i) churn flow ($j_G = 12.7$ m/s, $j_L = 1.0$ m/s); (j) churn flow ($j_G = 31$ m/s, $j_L = 0.51$ m/s); (k) annular flow ($j_G = 21.5$ m/s, $j_L = 0.02$ m/s).

a result, the nose of the bubble was more elongated while the rear part turned to be more flattened (Edvinsson and Irandoust, 1996; Kreutzer et al., 2005b), as shown in Fig. 3(d). Contrary to the phenomenon generally observed in large pipes, smaller bubbles were seldom seen in liquid slugs. (2) Unstable slug flow existed when j_G was relatively high. Under this circumstance, two adjacent bubbles were so close to each other that gas–liquid flow exhibited significant randomness (Fig. 3(e)). The rupture of an extremely longer bubble could be seen in some occasions (Fig. 3(f)) while sometimes a specific flow pattern called 'bubble-train slug flow' (Chen et al., 2002) was also found (Fig. 3(g)).

Depending on the magnitude of j_L, different flow patterns would appear upon further increasing j_G in slug flow. Slug-annular flow occurred at relatively low j_L (Fig. 3(h)) while the build of churn flow with two different types (Figs. 3(i) and (j)) was seen at relatively high j_L. More detailed description about the two flow patterns can be found in our previous paper (Yue et al., 2007). Finally, an increase of j_G in slug-annular flow would lead to the formation of annular flow (Fig. 3(k)).

3.2. Axial two-phase flow pattern evolution in microchannels

In SMC I, two-phase flow pattern formed at the entrance may evolve gradually along the main microchannel due to the interaction between two competitive factors. On the one hand, relatively high pressure drop experienced in the microchannel will cause gas density to decrease from the entrance till the end; on the other hand, mass transfer process accompanying CO_2–water flow will lead to the absorption of CO_2 into water simultaneously, which contributes to a decrease of the gas mass flow rate along the microchannel. Consequently, it is expected that under some specific conditions, there will be a relatively big change in the superficial gas velocity along the microchannel so that different flow patterns may exist at the entrance and in the middle section of the microchannel, respectively.

Take Taylor flow as an example, the gas compressibility will cause an increase in Taylor bubble length along the microchannel (Taitel and Barnea, 1998) while the gas absorption process will cause a decrease in Taylor bubble length. Figs. 4(a)–(c) show the comparison between the ratios of Taylor bubble length to the hydraulic diameter measured at the entrance and in the middle section of the microchannel for three contactors, respectively. The uncertainty in the measured (L_B/d_h) in both locations was estimated to be about 8% according to error analysis theory (Moffat, 1988) and the corresponding uncertainty bars were also depicted in these figures. It can be seen from Fig. 4(a) that for the biggest microchannel with $d_h = 667\,\mu m$, Taylor bubble length in the middle section is always much lower than that at the entrance. The observed significant axial reduction of Taylor bubble length may be attributed to the dominance of mass transfer effect over the gas compressibility effect in this microchannel, which is further verified by our previous mass transfer experiments (Yue et al., 2007). In detail, it was found that two-phase total pressure drop associated with Taylor flow was relatively small (usually on the order of several kPa) as compared to the absolute pressure

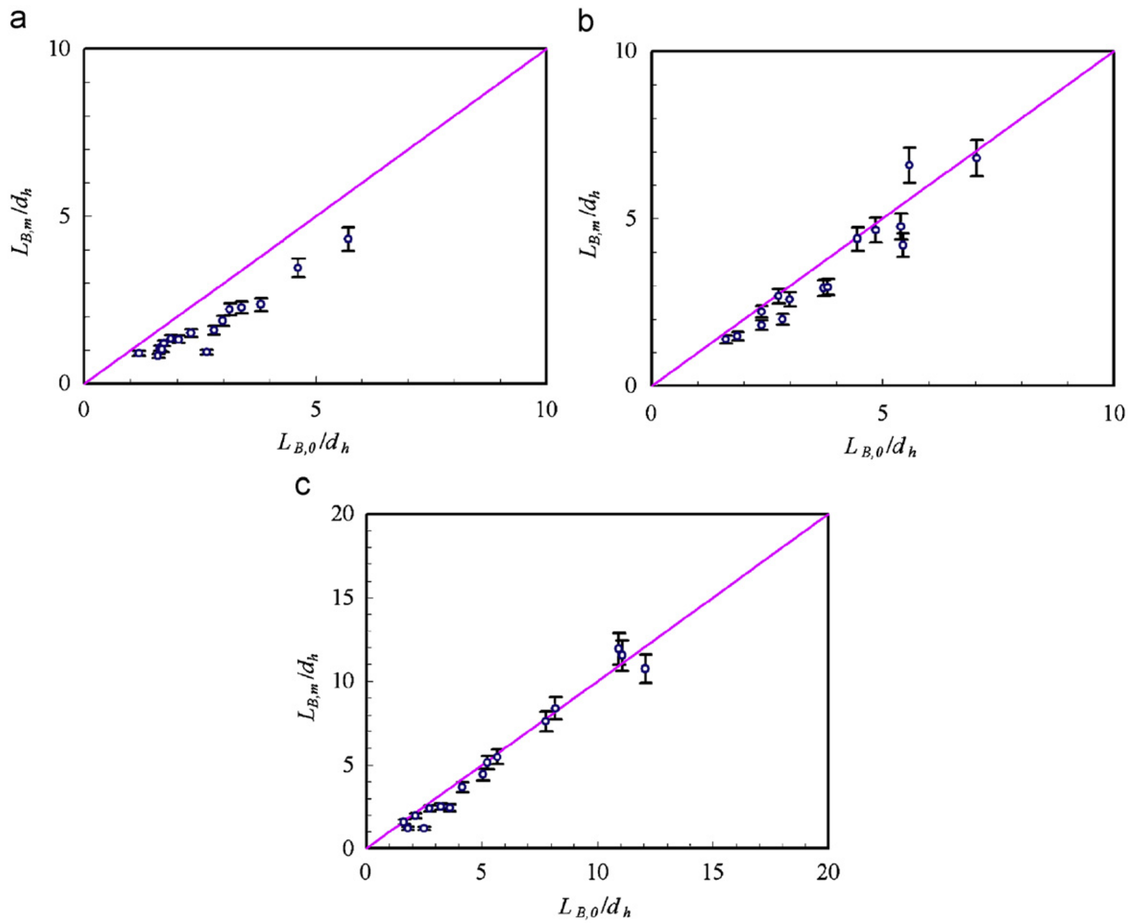

Fig. 4. Comparison between the ratios of Taylor bubble length to the hydraulic diameter measured at the entrance and in the middle section of the microchannel: (a) $d_h = 667\,\mu m$; (b) $d_h = 400\,\mu m$; (c) $d_h = 200\,\mu m$.

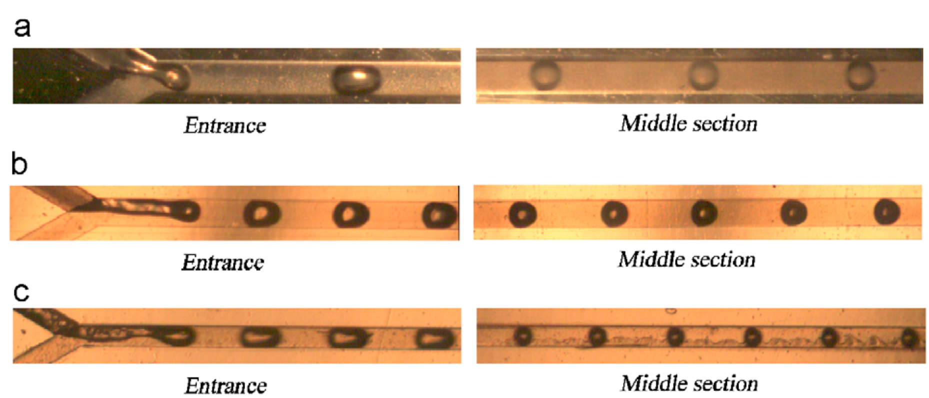

Fig. 5. Two-phase flow pattern evolution along the microchannel: (a) $d_h = 667\,\mu m$, $j_{G,0} = 0.089$ m/s, $j_L = 0.50$ m/s; (b) $d_h = 400\,\mu m$, $j_{G,0} = 0.29$ m/s, $j_L = 0.51$ m/s; (c) $d_h = 200\,\mu m$, $j_{G,0} = 0.40$ m/s, $j_L = 0.54$ m/s.

measured in this microchannel while the amount of gas absorption was somewhat remarkable. Thus, the gas compressibility effect was insignificant and Taylor bubble length was gradually reduced along the microchannel due to the accompanying gas absorption process. For the other two smaller microchannels, the comparisons shown in Figs. 4(b) and (c) indicate that the axial reduction in Taylor bubble length occurred when the formed Taylor bubble at the entrance was relatively short, implying that mass transfer effect was also important under such circumstance. However, an axial increase in Taylor bubble length seemed to exist when the formed Taylor bubble at the entrance was very long. Perhaps, the gas compressibility effect was more significant in this case, which needs to be clarified in our future work since mass transfer data in these two microchannels have not been obtained as yet. Based on the above observations, one may further imagine that if the operational condition is set such that a Taylor flow containing very short bubble lengths is produced at the entrance, two-phase flow pattern in the middle section will turn out to be bubbly flow. That is, the elongated Taylor bubble shrinks to a spherical bubble as a result of mass transfer process therein. As revealed in Fig. 5, the shift of flow pattern from Taylor flow to bubbly flow did occur under some critical operational conditions for all three microchannels investigated. This phenomenon should be fully considered during the investigation of mass transfer characteristics and reaction behavior under Taylor flow in microchannels.

3.3. Flow pattern maps for microchannels

Two-phase flow in microchannels features itself in the fact that under most circumstances, surface tension has an important role to play and laminar flow nature of each phase prevails. Therefore, a lot of widely used models and correlations for large pipes have been found to fail in describing flow pattern transition behavior in microchannels (Triplett et al., 1999a; Zhao and Bi, 2001a). New flow pattern maps with reasonable flow transition lines included are urgently needed, where the pioneer works of Triplett et al. (1999a) and Akbar et al. (2003) have been seen toward this direction.

Figs. 6(a)–(c) show the obtained flow pattern maps with the superficial gas and liquid velocities as coordinates for the present three microchannels. The whole data of bubbly flow and one part data of slug flow (i.e., Taylor flow sub-regime) in these figures were plotted according to the flow pattern pictures observed at the entrance of the microchannel due to somewhat high uncertainty in determining the superficial gas velocity in the middle section under these operational conditions. Therefore, these data were based on the superficial gas velocities calculated at the entrance. For the other flow patterns, data were depicted according to the pictures observed in the middle section of the microchannel and the superficial gas velocity was calculated in the same way as that shown in Fig. 3. In the smallest microchannel with $d_h = 200\,\mu$m, experiments were conducted within relatively short operational ranges due to much higher pressure drop encountered in this microchannel.

Generally, slug flow dominated at low and moderate j_G while bubbly flow only occurred at extremely low j_G and very high j_L. In the microchannels with $d_h = 667$ and $200\,\mu$m, slug-annular flow was not detected at the lowest j_L. Maybe under these circumstances it was difficult to discern this flow pattern from annular flow. Another phenomenon noted was that stratified flow was never seen in our experiments, which has already been confirmed by many authors (Chung and Kawaji, 2004; Serizawa et al., 2002; Triplett et al., 1999a). The precise condition for stratified flow to occur in microchannels is still not known at present.

In Figs. 6(a)–(c), the flow transition lines proposed by Triplett et al. (1999a) for a 1.097 mm diameter circular microchannel are included for comparison. For the microchannel with $d_h = 667\,\mu$m, the predictions of Triplett et al. (1999a) are generally in good agreement with the experimental observations over all flow transitions. For the microchannel with $d_h = 400\,\mu$m, the transitions from slug flow to slug-annular flow and from slug-annular flow to annular flow can be well represented by their predictions. However, the poorest agreement has been found in the smallest microchannel with $d_h = 200\,\mu$m, as shown by the significant deviations of the flow transition lines proposed by Triplett et al. (1999a) from all available transitional boundaries measured in this microchannel.

Consequently, empirical correlations solely based on the superficial gas and liquid velocities are not adequate to interpret flow pattern transition behavior in microchannels with different diameters. More parameters which turn to be important in microchannels should be incorporated into these correlations. Thus, flow transition correlations based on dimensionless groups such as those proposed by Akbar et al. (2003) seem to be more reasonable. Akbar et al. (2003) suggested that there is an important resemblance between two-phase flow in microchannels and those in large channels at microgravity. Based on the work of Rezkallah (1996) who has found that the flow transition lines for gas–liquid two-phase flow at microgravity could be expressed approximately as $We_{GS} \propto We_{LS}^{0.25}$, Akbar et al. (2003) divided the entire flow pattern map for microchannels into four zones (surface tension-dominated zone, transition zone, annular flow zone and dispersed flow zone) among which the transition boundaries were also represented using We_{GS} and We_{LS} as coordinates. Recently, the experimental data of Chen et al. (2006) also indicate that the superficial Weber numbers may be the right parameter to predict the transition boundaries in microchannels that include the effect of diameter.

The comparison between our experimental data and the transition lines proposed by Akbar et al. (2003) were shown in the flow

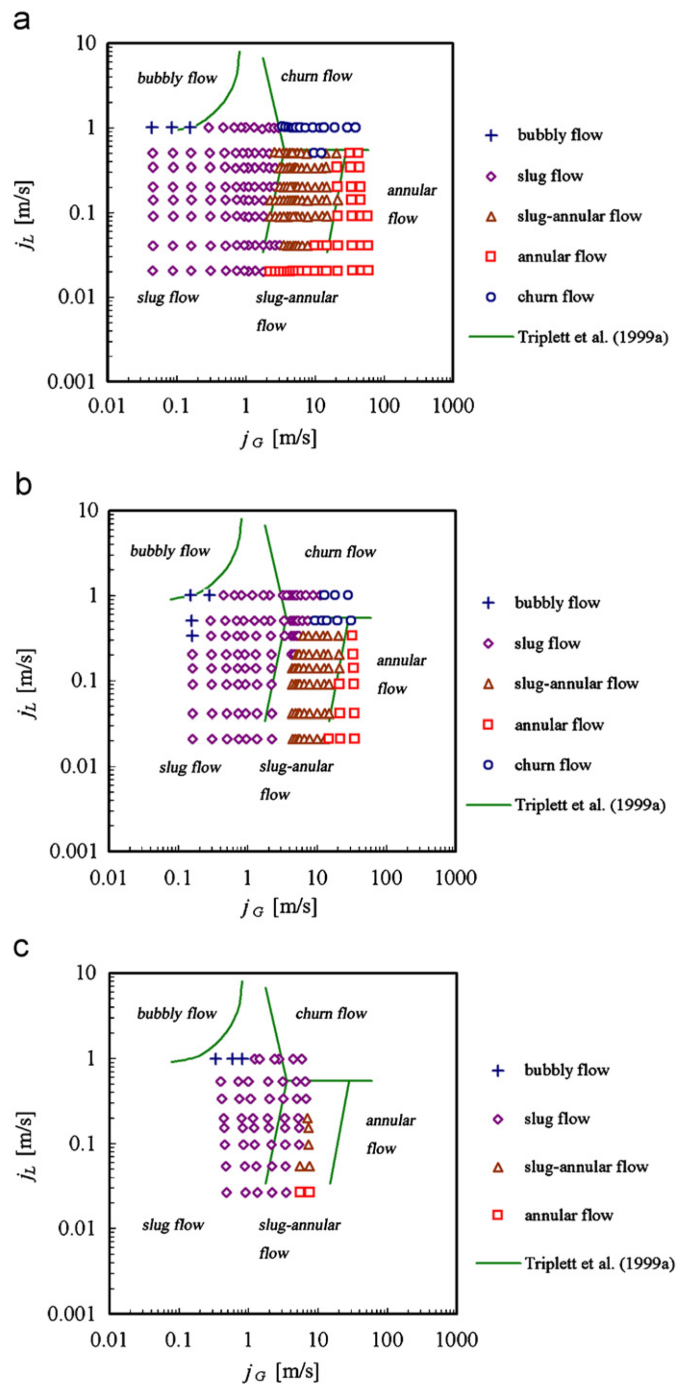

Fig. 6. Flow pattern maps for the present microchannels using the superficial gas and liquid velocities as coordinates and comparison with the flow transition lines of Triplett et al. (1999a) for a 1.097 mm diameter circular microchannel: (a) $d_h = 667\,\mu$m; (b) $d_h = 400\,\mu$m; (c) $d_h = 200\,\mu$m.

pattern maps with We_{GS} and We_{LS} as coordinates (Figs. 7(a)–(c)). It should be noted that here Taylor flow and unstable slug flow were shown separately as a sub-regime of slug flow. Obviously, the correlations of Akbar et al. (2003) enjoy large success in the prediction of all flow transitions among the above-mentioned four zones in the microchannel with $d_h = 667\,\mu m$ except at the lowest We_{LS} where slug-annular flow was not observed in our experiments and at the highest We_{LS} where the deviation on the slug–churn transition is thought to be partly a result of the apparent inconsistency regarding the definition of churn flow among different authors (Yue et al., 2007). In the microchannel with $d_h = 400\,\mu m$, at least the transitions from slug flow to slug-annular flow, from slug-annular flow to annular flow and from slug flow to churn flow at the highest We_{LS} appear to be well represented by their predictions. As to the microchannel with $d_h = 200\,\mu m$, although the obtained data are somewhat scarce, it can be observed that the transition boundary between slug flow and slug-annular flow is not well described by their model. In conclusion, the correlations of Akbar et al. (2003) seems to be feasible in predicting two-phase flow transitions in microchannels, but much improvement is still needed. In the work of Akbar et al. (2003), bubbly–slug transition was not considered because the two flow patterns were included together into the surface tension-dominated zone. Here, an attempt of predicting this transition was not made due to the scarcity of data. However, the transition line from Taylor flow to unstable slug flow can be roughly represented by the following correlation:

$$We_{GS} = 0.0172 We_{LS}^{0.25} \qquad (4)$$

The exponent item associated with We_{LS} was simply assumed as 0.25 according to the findings of Rezkallah (1996). As revealed in Figs. 7(a)–(c), Eq. (4) compares favorably with the experimental data in all three microchannels. This correlation is very helpful for the operation of gas–liquid microreactors because Taylor flow is expected to have many advantages over other flow patterns with regard to mass transfer characteristics and reaction behavior.

3.4. Taylor flow in microchannels

Under typical conditions of interest for mass transfer operations and chemical reactions in gas–liquid microreactors, Taylor flow is the preferred flow pattern due to its distinguished advantages (Günther and Jensen, 2006; Kreutzer et al., 2005a). In this flow pattern, reduced axial mixing in liquid phase is anticipated due to the separation of the bulk liquid by bubbles with only very thin films connecting in between and improved radial mixing is achieved by the inner circulation in the liquid slug region that trails the bubble (Trachsel et al., 2005). Furthermore, the thin film region between the gas and the channel wall will facilitate mass transfer and reaction processes therein (Kreutzer et al., 2001; Vandu et al., 2005). Thus, it is very meaningful to investigate hydrodynamics of Taylor flow in microchannels in order to realize this flow in a highly controlled manner.

3.4.1. Taylor bubble formation mechanism

A survey in the open literature reveals that Taylor bubble formation mechanism in microchannels is highly dependent on the inlet configuration (Cubaud et al., 2005; Garstecki et al., 2005, 2006; Salman et al., 2006), which has a subsequent influence on the lengths of Taylor bubbles and liquid slugs formed at the entrance. Garstecki et al. (2006) have experimentally investigated the process of formation of droplets and bubbles in microfluidic T-junction geometries. They suggested that the break-up mechanism of the immiscible thread of the discontinuous fluid was mainly dependent on the relative magnitude of forces involved in this process, i.e., interfacial stress caused by surface tension, shear stress exerted on the tip of the discontinuous fluid by the continuous phase, resistance of flow to the

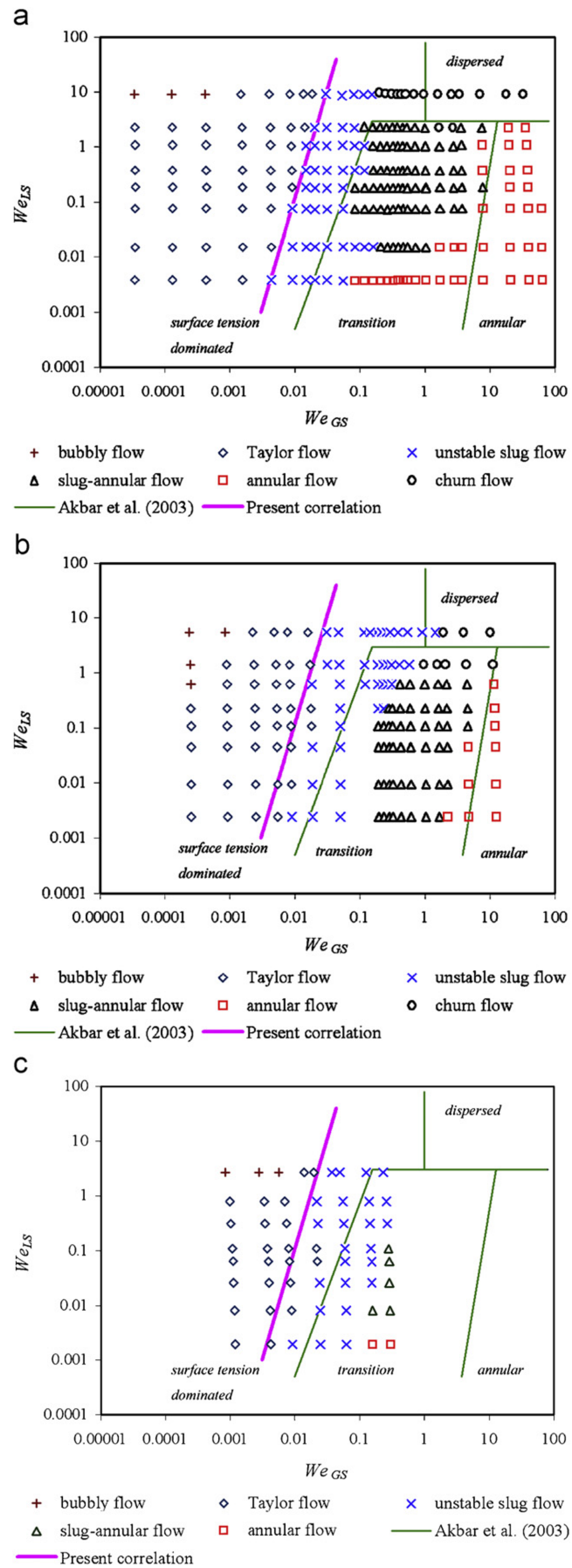

Fig. 7. Flow pattern maps for the present microchannels using the superficial Weber numbers as coordinates and comparison with the flow transition lines of Akbar et al. (2003): (a) $d_h = 667\,\mu m$; (b) $d_h = 400\,\mu m$; (c) $d_h = 200\,\mu m$.

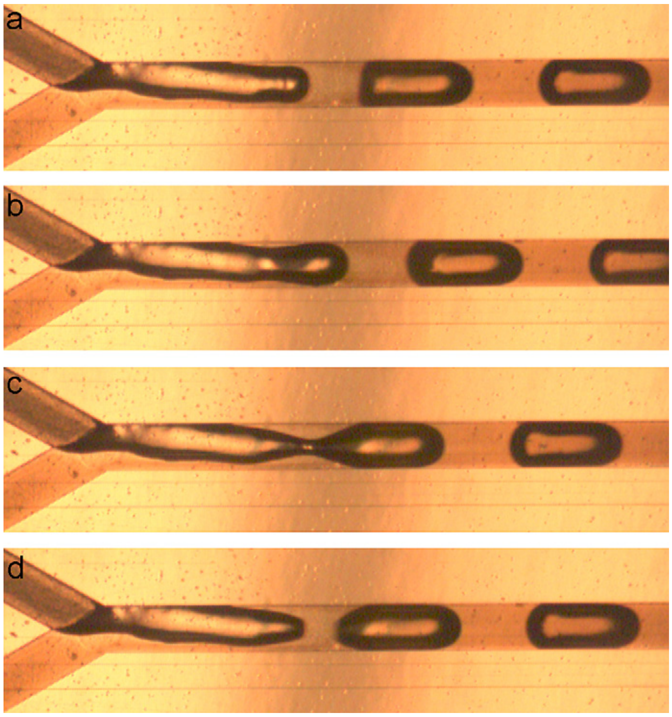

Fig. 8. Typical pictures of Taylor bubble formation process in the squeezing regime in the microchannel with $d_h = 400\,\mu m$ ($j_{G,0} = 0.48$ m/s, $j_L = 0.34$ m/s, $Ca = 0.011$): (a) Step 1; (b) Step 2; (c) Step 3; (d) Step 4.

continuous fluid resulted from the partially blockage of the cross-section of the main microchannel by the discontinuous fluid. When the leading contribution in the break-up dynamics was the force arising from the pressure drop across the emerging bubble or droplet, the break-up process was dominated by the squeezing mechanism. A simple scaling relation was then proposed to predict the length of Taylor bubble produced in this squeezing regime:

$$\frac{L_{B,0}}{W} = 1 + \alpha \frac{j_{G,0}}{j_L} \tag{5}$$

where α could be treated as a fitting parameter of order 1 and its particular value depended on the geometry of the T-junction. When the shear stress started to play an important role in the break-up process, the transition from the squeezing regime to the dripping regime would be expected, which mainly depended on the magnitude of Ca as well as the inlet geometry. Garstecki et al. (2006) observed that for T-junctions with $W/H \geqslant 1$ and $1 \leqslant W/W_{\text{in}} \leqslant 2$, the squeezing mechanism was expected to describe the break up at low values of Ca (typically $< 10^{-2}$). However, for the same Ca, an earlier transition to the dripping regime happened if the width of the main microchannel was much greater than that of the inlet microchannel ($W/W_{\text{in}} > 2$).

The present microchannel contactors contain Y-type junction geometries with an angle of 60° between side channels. Despite this slight modification, it was found that the above-mentioned two different mechanisms were also involved during the formation of Taylor bubbles in these microchannels.

The break-up process was found to be in the squeezing regime for all three microchannels at lower j_L, where Ca ranged from 0.0019 to 0.029. Fig. 8 shows a series of images taken during Taylor bubble formation in the microchannel with $d_h = 400\,\mu m$ ($Ca = 0.011$), which can be represented typically by four steps: (a) Step 1, two phases form an interface either locating at the inlet junction or further extending to a distance of several d_h downstream, from which gas continues to penetrate into the flowing liquid with a growing nearly hemispherical bubble tip; (b) Step 2, the bubble shape becomes elongated and begins to block almost the entire cross-section of the microchannel when the diameter of the bubble tip approaches the width of the microchannel; (c) Step 3, liquid pressure upstream the emerging bubble increases dramatically due to less available space for liquid passage, which leads to the squeezing of the gas neck; (d) Step 4, a Taylor bubble is produced after the break up of the gas neck and a new cycle repeats again. One significant feature observed in this squeezing regime is that the film formed between the emerging bubble and the wall is far less than the width of the microchannel and thus the force arising from the pressure drop across the emerging bubble is dominant in the break-up process (Garstecki et al., 2006).

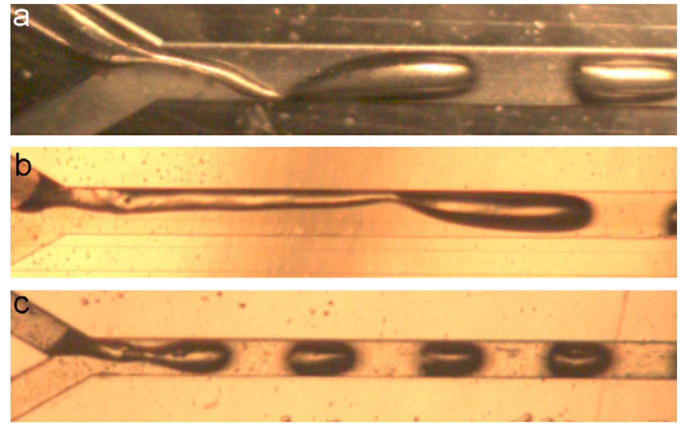

Fig. 9. Typical photographs observed during Taylor bubble formation in the dripping regime in three microchannels: (a) $d_h = 667\,\mu m$, $j_{G,0} = 0.68$ m/s, $j_L = 1.0$ m/s, $Ca = 0.023$; (b) $d_h = 400\,\mu m$, $j_{G,0} = 1.16$ m/s, $j_L = 1.0$ m/s, $Ca = 0.03$; (c) $d_h = 200\,\mu m$, $j_{G,0} = 1.23$ m/s, $j_L = 1.0$ m/s, $Ca = 0.031$.

The transition from the squeezing regime to the dripping regime was only found at the highest j_L of 1.0 m/s in three microchannels, where Ca ranged from 0.017 to 0.034. Some typical images were demonstrated in Fig. 9. It is obvious that the emerging bubble in this regime only blocks part of the microchannel cross-section. As a result, under this circumstance the main driving force for the pinch of the thread turns to be shear stress or a combination of shear stress and the force associated with the build-up of pressure upstream of the emerging bubble (Garstecki et al., 2006). The detached Taylor bubble will transform slightly in order to reoccupy nearly the entire cross-section of the microchannel when further moving downstream. It can be seen from Fig. 9 that the effective gas inlet width (i.e., the gas neck width right at the beginning of the main microchannel) is much less than the width of the main microchannel. Consequently, a transition to the dripping regime was observed, which is consistent with the findings of Garstecki et al. (2006) who noticed that besides Ca, W/W_{in} was another important parameter in this transition.

To examine the applicability of Eq. (5) for the prediction of Taylor bubble length in the squeezing regime, the currently obtained data were compared with the predictions of this equation in Fig. 10, where α was determined by the linear least square regression method. Generally Taylor bubble length can be well represented by Eq. (5) with a constant α. An identical value of α, 1.18, can be assigned for the two square microchannels while a higher value of α, 2.71, is achieved for the rectangular microchannel with $d_h = 667\,\mu m$. According to the analysis of Garstecki et al. (2006), α can be roughly treated as the ratio between the characteristic width of the neck at the time when the discontinuous phase fully enters the main microchannel and W. For the two square microchannels, the neck was thought to assume a circular cross-section and its diameter was comparable to the width of the microchannel when the bubble began to span almost the

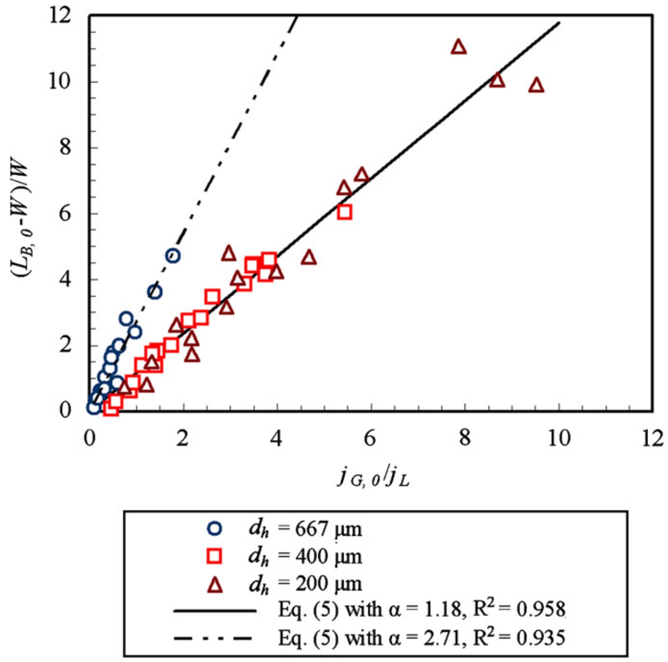

Fig. 10. Comparison between the measured Taylor bubble lengths in three microchannels in the squeezing regime and those predicted by Eq. (5) ($0.046 \leqslant j_{G,0} \leqslant 1.2$ m/s, $0.02 \leqslant j_L \leqslant 0.54$ m/s, $0.0019 \leqslant Ca \leqslant 0.029$).

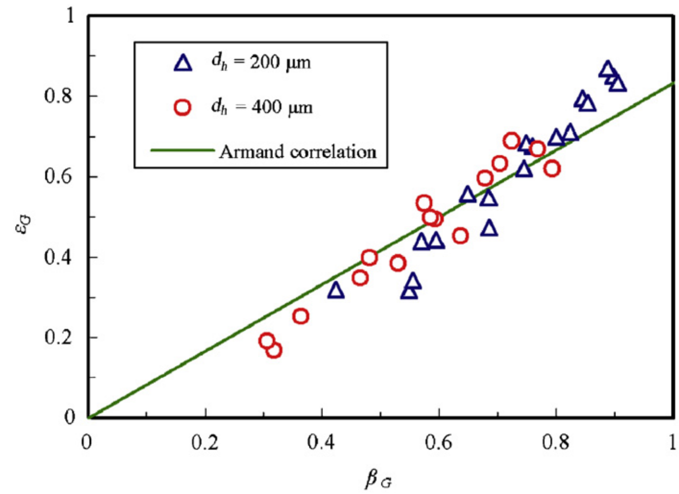

Fig. 11. Measured gas hold up data and the predictions of the Armand correlation versus gas volumetric fraction for Taylor flow in the microchannels with $d_h = 200$ and 400 μm.

entire cross-section of the microchannel (see Fig. 8(b)), which means that in this case α in Eq. (5) should be close to 1. The obtained somewhat higher value of α, 1.18, is possible since not all the flow rate of liquid contributes to squeezing and the speed at which the neck collapses need not to be constant (Garstecki et al., 2006). For the rectangular microchannel with $d_h = 667$ μm, the cross-section of the neck cannot be regarded as circular due to the higher aspect ratio of 2 therein. Here, the characteristic dimension of the neck was thought to be much higher than the width of the microchannel and therefore a higher value of 2.71 was obtained for the constant α by the fitting procedure. To further elucidate the effect of aspect ratio on the Taylor bubble formation in rectangular microchannels, detailed experiments and simulation work are still necessary.

3.4.2. Gas hold up

Many authors have found that the following Armand correlation represents gas hold up data well for Taylor flow of air–water like fluid pairs in microchannels (Chung and Kawaji, 2004; Serizawa et al., 2002; Zhao and Bi, 2001b),

$$\varepsilon_G = 0.833\beta_G \tag{6}$$

where $\beta_G = j_G/(j_G + j_L)$.

The gas hold up data in Taylor flow observed near the entrance of the present two square microchannels with $d_h = 400$ and 200 μm were calculated on the basis of the assumptions that the front and rear parts of a Taylor bubble were hemispherical with their diameters equal to the channel width and that the film thickness was negligible. Therefore, it is obtained upon reduction that

$$\varepsilon_G = \frac{L_{B,0}}{L_{B,0} + L_{S,0}} + \left(\frac{\pi}{6} - 1\right)\frac{W}{L_{B,0} + L_{S,0}} \tag{7}$$

The hold up data obtained in such way as a function of β_G are compared with those predicted by Eq. (6) in Fig. 11. Again it seems that the Armand correlation can give a reasonable prediction of gas hold up in Taylor flow through square microchannels. For the rectangular microchannel with $d_h = 667$ μm, the high aspect ratio may cause the front and rear parts of a Taylor bubble to deviate much from ideal hemispheroids and bring up inconstant film thickness on all four sides of the channel, causing somewhat high calculation complexity. Therefore, the validity of the Armand correlation was not examined in this microchannel.

3.5. Pressure drop characteristics

For gas–liquid two-phase flow in large pipes, most of the available pressure drop correlations are based on the traditional homogeneous flow model or separated flow model. In the homogeneous flow model, two phases are assumed to be thoroughly mixed and thus two-phase frictional pressure drop can be calculated from the formulas employed in single phase flow case based on the average properties of two-phase mixture. Therefore, a lot of two-phase mixture viscosity correlations have been suggested, making the selection of such correlations crucial for the successful application of this model (Wong and Ooi, 1995). In the separated flow model, gas and liquid are assumed to flow separately in the pipe with each phase occupying a sector of the pipe cross-section. A representative work was that of Lockhart and Martinelli (1949) in which two-phase frictional pressure drop can be derived from the significant relationship between two-phase frictional multiplier, Φ_L^2, and the Martinelli parameter, X. That is,

$$\left(\frac{\Delta P_F}{L}\right)_{TP} = \Phi_L^2\left(\frac{\Delta P_F}{L}\right)_L \tag{8}$$

$$X^2 = \frac{(\Delta P_F/L)_L}{(\Delta P_F/L)_G} \tag{9}$$

Here $(\Delta P_F/L)_L$ and $(\Delta P_F/L)_G$ are the frictional pressure drop gradients which would exist if liquid or gas flows alone in the pipe, respectively. Lockhart and Martinelli (1949) postulated that Φ_L^2 was a unique function of X, which was later supported by theoretical analyses of many authors on idealized stratified flow and annular flow in pipes (Chen and Spedding, 1981; Chisholm, 1967; Taitel and Dukler, 1976).

According to two-phase flow patterns observed in the present microchannels, it indicates that the homogeneous flow model may be only applicable to bubbly flow in which the liquid flow field is thought to be less disturbed by the presence of small bubbles, thus two-phase frictional pressure drop in this flow pattern can be described by correlations for single phase liquid flow if a proper expression for the mixture viscosity is chosen (Cubaud and Ho, 2004; Liu et al., 2005; Triplett et al., 1999b). However, the deviation from the homogenous flow assumption can be seen in Taylor flow. As revealed by Liu et al. (2005), there existed significant relative velocity between gas and liquid at lower superficial liquid velocities for air–ethanol Taylor flow in a square capillary with $d_h = 2.89$ mm. Meanwhile, Taylor flow cannot be regarded as a separated flow due to the alternate movement of Taylor bubbles and liquid slugs down the channel. Actually this flow pattern was eliminated from consideration in the separated flow model (Lockhart and Martinelli, 1949). Consequently, detailed flow analysis should be performed in order to formulate reasonable correlations for the prediction of pressure drop in this flow pattern (Garimella et al., 2002; Kreutzer et al., 2005b). As to flow patterns such as slug-annular flow, churn flow and annular flow, the separated flow model seems to be more realistic because the two-phase interface configuration in these flow patterns is close to the model assumption. In other words, under these flow patterns a continuous gas flow is seen in the center part of the microchannel while liquid film flows adjacent to the microchannel wall.

In the current setup, two-phase total pressure drop in the main microchannel, ΔP_T, can be roughly measured by using SMC I and SMC II shown in Figs. 1(a) and (b), respectively. As described above, the gas mass flow rate cannot be considered as constant along the main microchannel for bubbly flow and Taylor flow due to significant mass transfer effect therein, which made it difficult to develop suitable pressure drop correlations for these flow patterns based on the available data. Hence, in this section, we only deal with pressure drop data obtained in flow patterns including churn flow, slug-annular flow and annular flow. The average pressure between the main microchannel entrance and outlet was used to derive j_G appearing hereafter. Also, it should be noted that a few pressure drop data in the microchannels with $d_h = 667$ and 400 μm were collected under the condition that gas flow may be turbulent ($Re_{GS} > 1300$) and are not considered here.

Two-phase frictional pressure drop gradient in the main microchannel can be calculated as

$$\left(\frac{\Delta P_F}{L}\right)_{TP} = \frac{\Delta P_T - \Delta P_A}{L} \tag{10}$$

where

$$\Delta P_A = G^2\left[\left(\frac{x^2}{\rho_G \varepsilon_G} + \frac{(1-x)^2}{(1-\varepsilon_G)\rho_L}\right)_1 - \left(\frac{x^2}{\rho_G \varepsilon_G} + \frac{(1-x)^2}{(1-\varepsilon_G)\rho_L}\right)_0\right] \tag{11}$$

Here the Armand correlation, Eq. (6), is further extrapolated to flow patterns other than Taylor flow with the aim of an approximate estimation of ΔP_A. This treatment will not cause much error in the obtained two-phase frictional pressured drop data, as can be seen from the result that under our experimental conditions, ΔP_A thus obtained was very small compared with ΔP_T (generally lower than 3% of the latter in three microchannels).

In view of the fact that the separated flow model is more suitable for a reasonable explanation of pressure drop characteristics in flow patterns such as slug-annular flow, churn flow and annular flow, we first compare the obtained data with the predictions based on this model. For engineering calculations, Chisholm (1967) recommended the following equation for the prediction of Φ_L^2:

$$\Phi_L^2 = 1 + \frac{C}{X} + \frac{1}{X^2} \tag{12}$$

Figs. 12(a) and (b) plot the evolutions of the measured Φ_L^2 in these flow patterns as a function of X in two microchannels with $d_h = 667$ and 400 μm, respectively. As Re_{GS} and Re_{LS} involved in these figures are well below a value of 2000, both gas and liquid flow in these microchannels were thought to be in the laminar regime. Thus, according to the suggestion of Chisholm (1967), C value in Eq. (12) can be taken as 5. However, it can be observed from the comparisons made in Figs. 12(a) and (b) that the current data are not well represented by Chisholm equation (12) with a single C value of 5. Furthermore, at a fixed X, there are a series of values of Φ_L^2 depending on the magnitude of j_L. Thus under these circumstances Φ_L^2 cannot be expressed as a unique function of X due to the presence of the significant effect of j_L on Φ_L^2. For ideal annular flow in pipes, a rather simple correlation between Φ_L^2 and ε_L could be found (Chisholm, 1967; Chen and Spedding, 1981). For example, it was shown by Chisholm (1967) that under the condition of laminar flows of gas and liquid in a pipe, there should be

$$\Phi_L^2 = \varepsilon_L^{-2} \tag{13}$$

Also in this case, we have

$$X = \sqrt{\frac{\mu_L j_L}{\mu_G j_G}} \tag{14}$$

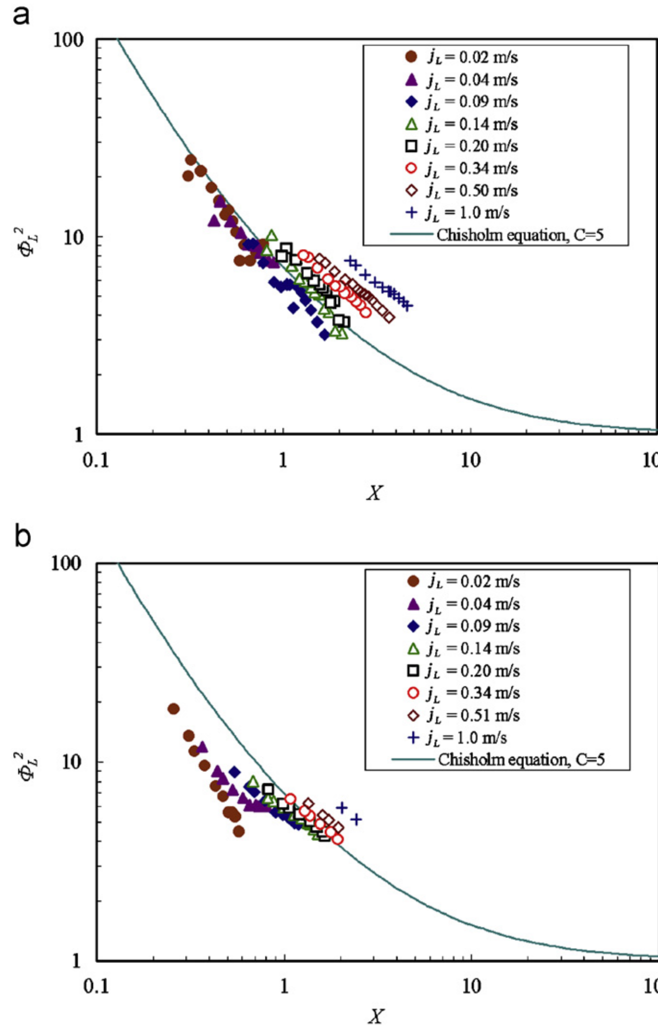

Fig. 12. Evolution of the measured Φ_L^2 as a function of X under flow patterns including slug-annular flow, annular flow and churn flow in microchannels: (a) $d_h = 667$ μm, $187 < Re_{GS} < 1262$, $13 < Re_{LS} < 701$; (b) $d_h = 400$ μm, $221 < Re_{GS} < 1101$, $8 < Re_{LS} < 396$.

Table 2
Comparison between values of Φ_L^2 calculated from Chisholm equation (12) and Eq. (15) for air–water two-phase flow in pipes at ambient conditions (20 °C, 101 kPa)

β_L	0.001	0.002	0.004	0.006	0.008	0.01	0.04	0.06	0.08	0.1
X	0.236	0.333	0.472	0.578	0.668	0.748	1.52	1.88	2.2	2.48
Φ_L^2 from Eq. (12) with $C=5$	40.3	25	16.1	12.6	10.7	9.47	4.72	3.94	3.49	3.18
Φ_L^2 from Eq. (15)	31.6	22.4	15.8	12.9	11.2	10	5	4.08	3.54	3.16

Hence, the key to a successful application of Lockhart–Martinelli approach to a large extent depends on whether ε_L is a unique function of the Martinelli parameter, X. During slug-annular flow, churn flow and annular flow in a rectangular microchannel, Eq. (13) is thought to be approximately applicable if the same assumptions as those of Chisholm (1967) are adopted. However, the non-circular cross-sectional geometry may lead to the significant velocity slip at gas–liquid interface and the retention of significant amounts of liquid inside four corners of the channel which is hard to be blown off under a wide range of operational conditions. As a result, ε_L is expected to be more sensitive to the change in j_L than that in j_G, which indicates that a simple correlation of ε_L solely based on X cannot be developed under these flow patterns in a rectangular microchannel. This may explain why the significant effect of j_L on the measured Φ_L^2 has been observed in the present microchannels. Thus, Lockhart–Martinelli method cannot be adopted directly without proper modifications.

Cubaud and Ho (2004) have performed experiments of air–water flow in two square microchannels with $d_h = 200$ and $525\,\mu$m, respectively. They found that at small liquid volumetric fraction ($0.001 < \beta_L < 0.1$) where annular flow was the dominant flow pattern, Φ_L^2 can be described by the following equation:

$$\Phi_L^2 = \beta_L^{-1/2} \tag{15}$$

where $\beta_L = j_L/(j_G + j_L)$. The derivation of Eq. (15) is based on an analogy with the corresponding equation in the homogeneous flow model in which two-phase viscosity is assumed to be equal to that of the liquid. Unfortunately, Cubaud and Ho (2004) also pointed out that Eq. (15) better fitted their data only at high j_L. Therefore, the effect of j_L on Φ_L^2 is not fully represented by this equation. In fact, Eq. (15) is more suitable for the description of pressure drop characteristics encountered during two-phase flow of air–water like fluid pairs in large diameter pipes at ambient conditions. As shown by the comparison listed in Table 2, at such small liquid volumetric fractions, most values of Φ_L^2 calculated from Eq. (15) are very close to those predicted by Chisholm equation (12) with $C = 5$. Therefore, a simple modification of Eq. (15) is performed here in order to better explain the observed effect of j_L on the measured Φ_L^2 in the present microchannels. For the square microchannel with $d_h = 400\,\mu$m, the following correlation is proposed:

$$\Phi_L^2 = 0.217\beta_L^{-1/2} Re_{LS}^{0.3} \tag{16}$$

The constant and the exponent associated with Re_{LS} at the right side of Eq. (16) were derived based on the linear least square regression analysis of the obtained data. Fig. 13(a) displays the good predicting performance of this equation, where the standard deviation is only 9.68%. In Fig. 13(b) the validity of Eq. (16) for the prediction of Φ_L^2 in square microchannel geometries seems to be further corroborated by a few data already obtained in the microchannel with $d_h = 200\,\mu$m. As to the microchannel with $d_h = 667\,\mu$m, Eq. (16) cannot be applied directly due to the inherently higher aspect ratio in this case. However, the influence of aspect ratio on Φ_L^2 in this microchannel can be resolved by simply placing a different constant in Eq. (16). That is,

$$\Phi_L^2 = 0.284\beta_L^{-1/2} Re_{LS}^{0.3} \tag{17}$$

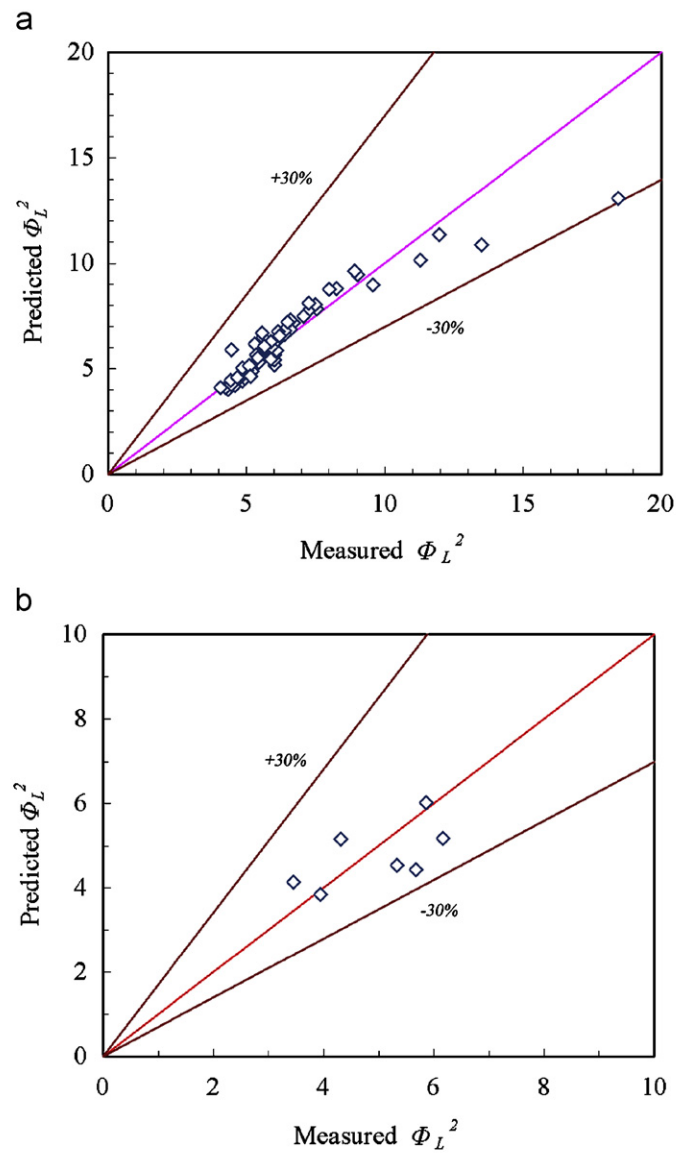

Fig. 13. Comparison between Φ_L^2 measured in flow patterns including slug-annular flow, annular flow and churn flow in two square microchannels and those predicted by Eq. (16): (a) $d_h = 400\,\mu$m, $221 < Re_{GS} < 1101$, $8 < Re_{LS} < 396$; (b) $d_h = 200\,\mu$m, $142 < Re_{GS} < 197$, $5 < Re_{LS} < 40$.

The comparison between the measured Φ_L^2 and that predicted by Eq. (17) for the microchannel with $d_h = 667\,\mu$m is shown in Fig. 14, where a small standard deviation of 21.5% was also achieved. To obtain a more universal correlation that can predict Φ_L^2 in rectangular microchannels, more experiments addressing the effects of fluid properties (surface tension, viscosity, etc.), hydraulic diameter and aspect ratio are needed to be conducted. The current data are still insufficient for such purpose.

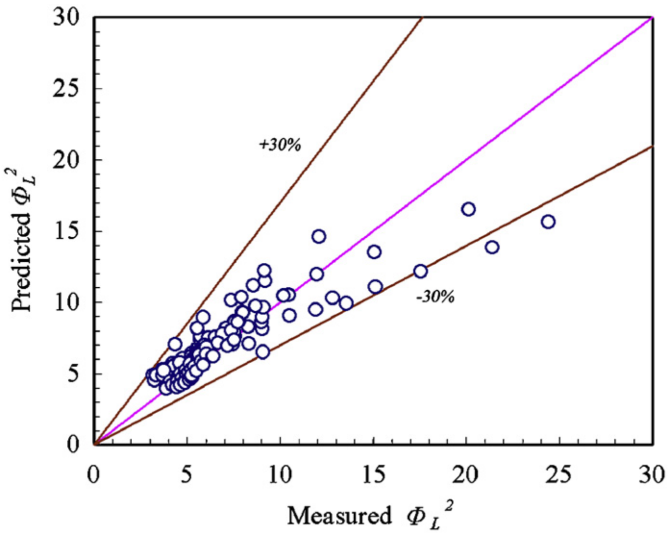

Fig. 14. Comparison between Φ_L^2 measured in flow patterns including slug-annular flow, annular flow and churn flow in the microchannel with $d_h = 667\,\mu$m and the predictions of Eq. (17) ($187 < Re_{GS} < 1262$, $13 < Re_{LS} < 701$).

4. Conclusions

Two-phase flow pattern and pressure drop characteristics during the absorption of CO_2 into water have been investigated in three horizontal single microchannel contactors which contain Y-type rectangular microchannels with hydraulic diameters of 667, 400 and 200 μm, respectively. The superficial velocities ranged from 0.04 to 60 m/s for the gas and 0.02 to 1.0 m/s for the liquid. Based on analyses and discussion presented in this paper, the following conclusions can be drawn:

(1) Flow patterns such as bubbly flow, slug flow (including two sub-regimes, Taylor flow and unstable slug flow), slug-annular flow, churn flow and annular flow were observed in the present microchannels. Flow pattern transition boundaries in the largest microchannel with $d_h = 667\,\mu$m were found to agree with the predictions of the flow transition lines proposed by Triplett et al. (1999a) and Akbar et al. (2003). However, the fitting performance of these lines becomes poor as the hydraulic diameter of the microchannel further reduces, which necessitates more work on the pursuit of a universal flow pattern map for microchannels. An empirical correlation based on the superficial Weber numbers, Eq. (4), has been developed to interpret the transition boundary between Taylor flow and unstable slug flow in the present three microchannels.

(2) Two mechanisms were found for the formation of Taylor bubbles in the current Y-junction microchannel geometries. At lower superficial liquid velocities where Ca ranged from 0.0019 to 0.029, Taylor bubble formation process was dominated by the squeezing mechanism while the transition to the dripping mechanism was observed at the highest superficial liquid velocity of 1.0 m/s. Lengths of Taylor bubbles formed in the squeezing regime can be well represented by the simple scaling relation proposed by Garstecki et al. (2006), i.e., Eq. (5). The measured gas hold up data under both regimes for two square microchannels with $d_h = 400$ and 200 μm can be approximately estimated by the Armand correlation.

(3) Two-phase frictional pressure drop in microchannels should be described by different models depending on the flow pattern investigated. For flow patterns such as slug-annular flow, annular flow and churn flow, the traditional separated flow model is more realistic. However, a significant effect of the superficial liquid velocity on the measured two-phase frictional multiplier was observed in the present microchannels, which was thought to be mainly a result of the complex relationship between liquid hold up and the superficial velocities of gas and liquid present in rectangular or square microchannels. Based on the experimental data, a reasonable correlation, Eq. (16), that can predict two-phase frictional multiplier using liquid volumetric fraction and the superficial liquid Reynolds number was proposed for microchannels with square cross-sections. Also, Eq. (17) with a different constant when compared to Eq. (16) was suggested for the microchannel $d_h = 667\,\mu$m in order to better fit the obtained data in this microchannel with a higher aspect ratio. For the complete resolution of the influence of aspect ratio on two-phase frictional multiplier, more systematic studies are required.

Notation

C	coefficient in Chisholm equation, Eq. (12)
Ca	capillary number defined by $(=\mu_L(j_G+j_L)/\sigma)$, dimensionless
d_h	hydraulic diameter, m
G	mass flux defined by $(=j_G\rho_G + j_L\rho_L)$, kg/(m^2 s)
H	height of the main microchannel, m
j	superficial velocity, m/s
L	length of the main microchannel, m
L_B	length of Taylor bubble, m
$L_{B,m}$	length of Taylor bubble in the middle section of the main microchannel, m
L_S	length of liquid slug, m
P	gauge pressure, Pa
$P_{\text{in, SMC I}}$	inlet gauge pressure in the gas feeding line during experiments with SMC I, Pa
$P_{\text{in, SMC II}}$	inlet gauge pressure in the gas feeding line during experiments with SMC II, Pa
ΔP_A	two-phase acceleration pressure drop, Pa
ΔP_F	frictional pressure drop, Pa
ΔP_T	two-phase total pressure drop, Pa
Re_{GS}	superficial gas Reynolds number defined by $(=d_h j_G \rho_G/\mu_G)$, dimensionless
Re_L	Reynolds number of liquid slug in Taylor flow defined by $(=d_h(j_G+j_L)\rho_L/\mu_L)$, dimensionless
Re_{LS}	superficial liquid Reynolds number defined by $(=d_h j_L \rho_L/\mu_L)$, dimensionless
W	width of the main microchannel, m
W_{in}	width of the side microchannel, m
We_{GS}	superficial gas Weber number defined by $(=d_h\rho_G j_G^2/\sigma)$, dimensionless
We_{LS}	superficial liquid Weber number defined by $(=d_h\rho_L j_L^2/\sigma)$, dimensionless
x	gas mass fraction
X	Martinelli parameter

Greek letters

α	fitting constant in Eq. (5)
β	phase volumetric fraction
ε	hold up
μ	viscosity, Pa s
ρ	density, kg/m^3
σ	surface tension, N/m
Φ_L^2	two-phase frictional multiplier

Subscripts

0	at the entrance of the main microchannel
1	at the outlet of the main microchannel
G	gas phase
L	liquid phase
TP	two-phase mixture

Acknowledgments

This work was supported by France ANR (Agence Nationale de la Recherche) within the "programme non thématique 2005" (No. NT05-3_41570), National Natural Science Foundation of China (No. 20490208), Foundation of the Ministry of Science and Technology (No. 2001CB711203 and No. 2006AA05Z233) and Fund of Dalian Institute of Chemical Physics, CAS (No. K2006D62).

References

Akbar, M.K., Plummer, D.A., Ghiaasiaan, S.M., 2003. On gas–liquid two-phase flow regimes in microchannels. International Journal of Multiphase Flow 29, 855–865.

Bi, Q.C., Zhao, T.S., 2001. Taylor bubbles in miniaturized circular and noncircular channels. International Journal of Multiphase Flow 27, 561–570.

Chen, J.J.J., Spedding, P.L., 1981. An extension of the Lockhart–Martinelli theory of two phase pressure drop and holdup. International Journal of Multiphase Flow 7, 659–675.

Chen, L., Tian, Y.S., Karayiannis, T.G., 2006. The effect of tube diameter on vertical two-phase flow regimes in small tubes. International Journal of Heat and Mass Transfer 49, 4220–4230.

Chen, W.L., Twu, M.C., Pan, C., 2002. Gas–liquid two-phase flow in micro-channels. International Journal of Multiphase Flow 28, 1235–1247.

Chisholm, D., 1967. A theoretical basis for the Lockhart–Martinelli correlation for two-phase flow. International Journal of Heat and Mass Transfer 10, 1767–1778.

Chung, P.M.-Y., Kawaji, M., 2004. The effect of channel diameter on adiabatic two-phase flow characteristics in microchannels. International Journal of Multiphase Flow 30, 735–761.

Cubaud, T., Ho, C.-M., 2004. Transport of bubbles in square microchannels. Physics of Fluids 16, 4575–4585.

Cubaud, T., Tatineni, M., Zhong, X., Ho, C.-M., 2005. Bubble dispenser in microfluidic devices. Physical Review E 72, 037302.

de Mas, N., Gunther, A., Schmidt, M.A., Jensen, K.F., 2003. Microfabricated multiphase reactors for the selective direct fluorination of aromatics. Industrial & Engineering Chemistry Research 42, 698–710.

Dukler, A.E., Wicks III, M., Cleveland, R.G., 1964. Frictional pressure drop in two-phase flow: B. An approach through similarity analysis. A.I.CH.E. Journal 10, 44–51.

Edvinsson, R.K., Irandoust, S., 1996. Finite-element analysis of Taylor flow. A.I.CH.E. Journal 42, 1815–1823.

Ehrfeld, W., Hessel, V., Löwe, H., 2000. Microreactors: New Technology for Modern Chemistry. Wiley-VCH, Weinheim.

Garimella, S., Killion, J.D., Coleman, J.W., 2002. An experimentally validated model for two-phase pressure drop in the intermittent flow regime for circular microchannels. Journal of Fluids Engineering 124, 205–214.

Garstecki, P., Stone, H.A., Whitesides, G.M., 2005. Mechanism for flow-rate controlled breakup in confined geometries: a route to monodisperse emulsions. Physical Review Letters 94, 164501.

Garstecki, P., Fuerstman, M.J., Stone, H.A., Whitesides, G.M., 2006. Formation of droplets and bubbles in a microfluidic T-junction—scaling and mechanism of break-up. Lab on a Chip 6, 437–446.

Günther, A., Jensen, K.F., 2006. Multiphase microfluidics: from flow characteristics to chemical and materials synthesis. Lab on a Chip 6, 1487–1503.

Hessel, V., Angeli, P., Gavriilidis, A., Löwe, H., 2005. Gas–liquid and gas–liquid–solid microstructured reactors: contacting principles and applications. Industrial & Engineering Chemistry Research 44, 9750–9769.

Inoue, T., Schmidt, M.A., Jensen, K.F., 2007. Microfabricated multiphase reactors for the direct synthesis of hydrogen peroxide from hydrogen and oxygen. Industrial & Engineering Chemistry Research 46, 1153–1160.

Jähnisch, K., Baerns, M., Hessel, V., Ehrfeld, W., Haverkamp, V., Löwe, H., Wille, Ch., Guber, A., 2000. Direct fluorination of toluene using elemental fluorine in gas/liquid microreactors. Journal of Fluorine Chemistry 105, 117–128.

Kawahara, A., Chung, P.M.-Y., Kawaji, M., 2002. Investigation of two-phase flow pattern, void fraction and pressure drop in a microchannel. International Journal of Multiphase Flow 28, 1411–1435.

Kobayashi, J., Mori, Y., Okamoto, K., Akiyama, R., Ueno, M., Kitamori, T., Kobayashi, S., 2004. A microfluidic device for conducting gas–liquid-solid hydrogenation reactions. Science 304, 1305–1308.

Kreutzer, M.T., Du, D., Heiszwolf, J.J., Kapteijn, F., Moulijn, J.A., 2001. Mass transfer characteristics of three-phase monolith reactors. Chemical Engineering Science 56, 6015–6023.

Kreutzer, M.T., Kapteijn, F., Moulijn, J.A., Heiszwolf, J.J., 2005a. Multiphase monolith reactors: chemical reaction engineering of segmented flow in microchannels. Chemical Engineering Science 60, 5895–5916.

Kreutzer, M.T., Kapteijn, F., Moulijn, J.A., Kleijn, C.R., Heiszwolf, J., 2005b. Inertial and interfacial effects on pressure drop of Taylor flow in capillaries. A.I.CH.E. Journal 51, 2428–2440.

Liu, H., Vandu, C.O., Krishna, R., 2005. Hydrodynamics of Taylor flow in vertical capillaries: flow regimes, bubble rise velocity, liquid slug length, and pressure drop. Industrial & Engineering Chemistry Research 44, 4884–4897.

Löb, P., Löwe, H., Hessel, V., 2004. Fluorinations, chlorinations and brominations of organic compounds in microreactors. Journal of Fluorine Chemistry 125, 1677–1694.

Lockhart, R.W., Martinelli, R.C., 1949. Proposed correlation of data for isothermal two-phase, two-component flow in pipes. Chemical Engineering Progress 45, 39–48.

Mcadams, W.H., 1954. Heat Transmission. third ed. McGraw-Hill, New York.

Moffat, R.J., 1988. Describing the uncertainties in experimental results. Experimental Thermal and Fluid Science 1, 3–17.

Rezkallah, K.S., 1996. Weber number based flow-pattern maps for liquid–gas flows at microgravity. International Journal of Multiphase Flow 22, 1265–1270.

Salman, W., Gavriilidis, A., Angeli, P., 2006. On the formation of Taylor bubbles in small tubes. Chemical Engineering Science 61, 6653–6666.

Serizawa, P.A., Feng, Z.P., Kawara, Z., 2002. Two-phase flow in microchannels. Experimental Thermal and Fluid Science 26, 703–714.

Taitel, Y., Barnea, D., 1998. Effect of gas compressibility on a slug tracking model. Chemical Engineering Science 53, 2089–2097.

Taitel, Y., Dukler, A.E., 1976. A theoretical approach to the Lockhart–Martinelli correlation for stratified flow. International Journal of Multiphase Flow 2, 591–595.

Tegrotenhuis, W.E., Cameron, R.J., Viswanathan, V.V., Wegeng, R.S., 2000. Solvent extraction and gas absorption using microchannel contactors. In: Ehrfeld, W. (Ed.), Microreaction Technology: Industrial Prospects: IMRET 3: Proceedings of the Third International Conference on Microreaction Technology. Springer, Berlin, pp. 541–549.

Trachsel, F., Günther, A., Khan, S., Jensen, K.F., 2005. Measurement of residence time distribution in microfluidic systems. Chemical Engineering Science 60, 5729–5737.

Triplett, K.A., Ghiaasiaan, S.M., Abdel-Khalik, S.I., Sadowski, D.L., 1999a. Gas–liquid two-phase flow in microchannels. Part I: two-phase flow patterns. International Journal of Multiphase Flow 25, 377–394.

Triplett, K.A., Ghiaasiaan, S.M., Abdel-Khalik, S.I., Lemouel, A., McCord, B.N., 1999b. Gas–liquid two-phase flow in microchannels. Part II: void fraction and pressure drop. International Journal of Multiphase Flow 25, 395–410.

Vandu, C.O., Liu, H., Krishna, R., 2005. Mass transfer from Taylor bubbles in single capillaries. Chemical Engineering Science 60, 6430–6437.

Wong, T.N., Ooi, K.T., 1995. Refrigerant flow in capillary tube: an assessment of the two-phase viscosity correlations on model prediction. International Communications in Heat and Mass Transfer 22, 595–604.

Yeong, K.K., Gavriilidis, A., Zapf, R., Hessel, V., 2004. Experimental studies of nitrobenzene hydrogenation in a microstructured falling film reactor. Chemical Engineering Science 59, 3491–3494.

Yue, J., Chen, G., Yuan, Q., 2004. Pressure drops of single and two-phase flows through T-type microchannel mixers. Chemical Engineering Journal 102, 11–24.

Yue, J., Chen, G., Yuan, Q., Luo, L., Gonthier, Y., 2007. Hydrodynamics and mass transfer characteristics in gas–liquid flow through a rectangular microchannel. Chemical Engineering Science 62, 2096–2108.

Zhao, T.S., Bi, Q.C., 2001a. Co-current air–water two-phase flow patterns in vertical triangular microchannels. International Journal of Multiphase Flow 27, 765–782.

Zhao, T.S., Bi, Q.C., 2001b. Pressure drop characteristics of gas–liquid two-phase flow in vertical miniature triangular channels. International Journal of Heat and Mass Transfer 44, 2523–2534.